
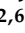



Article

# Angular Dependence of Copper Surface Damage Induced by an Intense Coherent THz Radiation Beam

Salvatore Macis <sup>1,2,\*</sup>, Luca Tomarchio <sup>1</sup>, Silvia Tofani <sup>3</sup> , S. Javad Rezvani <sup>2</sup>, Luigi Faillace <sup>4</sup>, Stefano Lupi <sup>1</sup>, Akinori Irizawa <sup>5</sup>  and Augusto Marcelli <sup>2,6</sup> 

<sup>1</sup> Department of Physics, Sapienza University, P.le Aldo Moro, 5, 00185 Roma, Italy; luca.tomarchio@uniroma1.it (L.T.); stefano.lupi@roma1.infn.it (S.L.)

<sup>2</sup> INFN, Laboratori Nazionali di Frascati, Via Enrico Fermi 40, 00044 Frascati (RM), Italy; javad.rezvani@lnf.infn.it (S.J.R.); augusto.marcelli@lnf.infn.it (A.M.)

<sup>3</sup> Department of Information Engineering, Electronics and Telecommunications, Sapienza University, Via Eudossiana, 18, 00184 Roma (RM), Italy; silvia.tofani@uniroma1.it

<sup>4</sup> INFN-Milano, Via Celoria 16, 20133 Milano, Italy; Luigi.Faillace@lnf.infn.it

<sup>5</sup> The Institute of Scientific and Industrial Research (ISIR), Osaka University, Osaka 565-0871, Japan; irizawa@sanken.osaka-u.ac.jp

<sup>6</sup> International Centre for Material Science Superstripes, RICMASS, Via dei Sabelli 119A, 00185 Rome, Italy

\* Correspondence: salvatore.macis@roma2.infn.it

Received: 26 January 2020; Accepted: 7 March 2020; Published: 10 March 2020



**Abstract:** In this work, we show the damage induced by an intense coherent terahertz (THz) beam on copper surfaces. The metallic surface was irradiated by multiple picosecond THz pulses generated by the Free Electron Laser (FEL) at the ISIR facility of the Osaka University, reaching an electric field on the sample surface up to  $\sim 4$  GV/m. No damage occurs at normal incidence, while images and spectroscopic analysis of the surface point out a clear dependence of the damage on the incidence angle, the electric field intensity, and polarization of the pulsed THz radiation. Ab initio analysis shows that the damage at high incidence angles could be related to the increase of the absorbance, i.e., to the increase of the temperature around or above 1000 °C. The experimental approach we introduced with multiple fast irradiations represents a new powerful technique useful to test, in a reproducible way, the damage induced by an intense electric gradient on copper and other metallic surfaces in view of future THz-based compact particle accelerators.

**Keywords:** THz; FEL; copper; damage; surface

## 1. Introduction

The damage induced by a strong EM field on metallic surfaces is a widely studied topic [1–3], where the aim is to understand the response of a material under strong applied electrical forces and the damage generated on the irradiated area. Experiments with intense electromagnetic radiation in the IR-UV range have been performed since the availability of high-intensity lasers [4,5]. Reflection and absorption processes of a high-intensity optical laser pulse by an extremely smooth metal surface have already been studied [5–8]. In particular, laser-induced damaged morphologies and their cumulative effects given by single pulses have already been highlighted [9].

The THz electromagnetic spectral range, typically referred to frequencies between 100 GHz and 10 THz, is fundamental for the spectroscopic analysis of many condensed matter systems [10–16], low dimensional semiconductors and superconducting materials with different electronic properties [17–20]. This frequency range is, in fact, resonant with molecular and phonon excitations and with free electrons in metals [21].

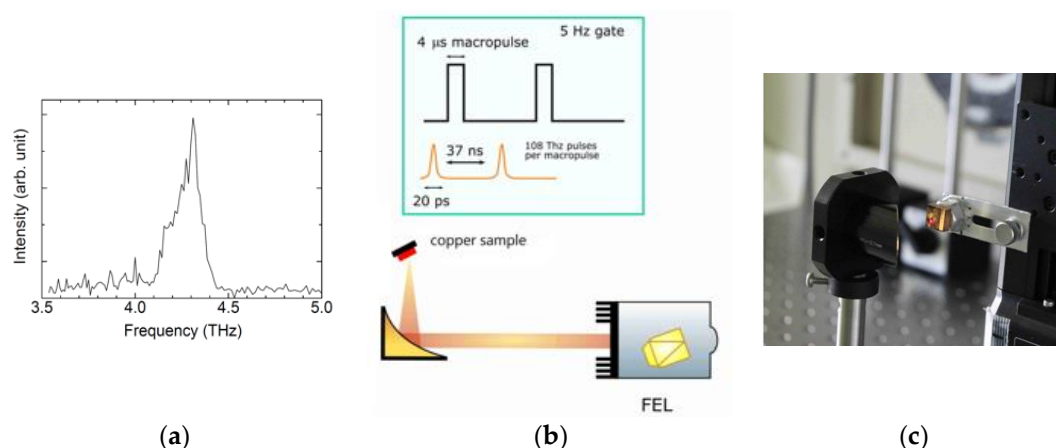
Despite its importance, the latest improvements in THz generation and detection have been hindered by the lack of suitable high-intensity sources. Recent developments have seen the appearance of optical techniques based on non-linear effects, like the optical rectification process in organic and inorganic crystals [22,23]. One of the most efficient ways to generate high-intensity THz pulses is based on relativistic electrons both in a Free Electron Laser (FEL) and a Linac, where the synchrotron radiation emission from the accelerated electron beam is coherent and (as for FELs) nearly monochromatic [13,14,24,25].

High-intensity THz radiation is also useful for producing a high-gradient electric field for particle acceleration [26]. The investigation of the behaviour of metallic cavities [27] under the application of a high-intensity THz field represents an important issue in the development of compact accelerators [22] and to test protective coatings designed to reduce the damaging processes [28,29]. Copper, in particular, represents a strategic material to study under high-gradient electric fields, due to its extensive use in many accelerating components subjected to high electric fields.

Recently Agranat et al. [9] investigated the damage induced on thin metallic films by a high-fluence pulsed THz radiation, while no irradiation studies have been performed on thick metallic samples yet. Here, we highlight the experimental results obtained by illuminating the surface of smooth copper thick samples with intense THz pulses generated at ISIR-FEL, a facility of the Osaka University [25], reaching an electric field on the sample surface up to  $\sim 4$  GV/m. Using multiple THz pulses, at the fluence below the single-pulse damage threshold, we show evidence of angular dependent damage of copper substrates. We analyze the damage through chemical analysis of the surface by Raman spectroscopy. We used a simple heat model coupled with Fresnel equations to explain the damaging mechanism taking into account the change of the surface reflectance vs. the incidence radiation angle.

## 2. Material and Methods

The THz-FEL at the quantum beam research facility of the Institute of Scientific and Industrial Research (ISIR) at the Osaka University allows the emission of nearly monochromatic coherent radiation through the acceleration of an electron beam by a LINAC up to 15 MeV. Electrons injected in the undulator emit horizontally polarized synchrotron radiation [25,30]. The optical system described in [25,31] allows the extraction of the coherent THz beam and its transport to the experimental hutch. Finally, the collimated beam is focused on the sample's surface through a parabolic mirror (Figure 1) sets at a distance of 5 cm.



**Figure 1.** (a) The spectrum of the FEL emission for an undulator gap of 37 mm, (b) layout and time structure of the THz pulses, (c) photo of the sample holder and of the parabolic mirror used to focus the radiation.

Knife-edge scanning measurements reveal the Gaussian profile of the beam at the focal point. The circular spot has a radius of  $\sim 130$   $\mu\text{m}$ , close to the diffraction limit [31]. Actually, the time structure

of the THz beam is related to the electron beam structure of the LINAC. By fixing the undulator gap at 37 mm, the narrow-band THz emission is centered at  $\sim 4.3$  THz. With a 5 Hz repetition rate, the time structure composed by a sequence of 4  $\mu\text{s}$  pulses is exploited. At the repetition rate of 27 MHz, each macro-pulse 20 ps long is composed of 108 micro-pulses. Figure 1a shows the typical frequency dispersion of this THz-FEL in the 27 MHz mode, reaching  $\sim 3\%$  bandwidth at the best monochromaticity conditions.

As measured by the calibrated energy meter (Multipurpose Energy Max Sensor J-25MB-LE form Coherent<sup>®</sup>) the FEL provides THz-pulse energy of  $4 \pm 0.1$  mJ on the sample surface. Considering an area with the size of the focus spot (130  $\mu\text{m}$  Gaussian radius), the fluence of the pulse on the sample surface is 12.7 J/cm<sup>2</sup>. At the focal point, a peak magnitude of 3.7 GV/m for the THz electric field has been evaluated using the equation:

$$E_{\text{THz}} = \sqrt{Z_0 I_{\text{THz}}} \quad (1)$$

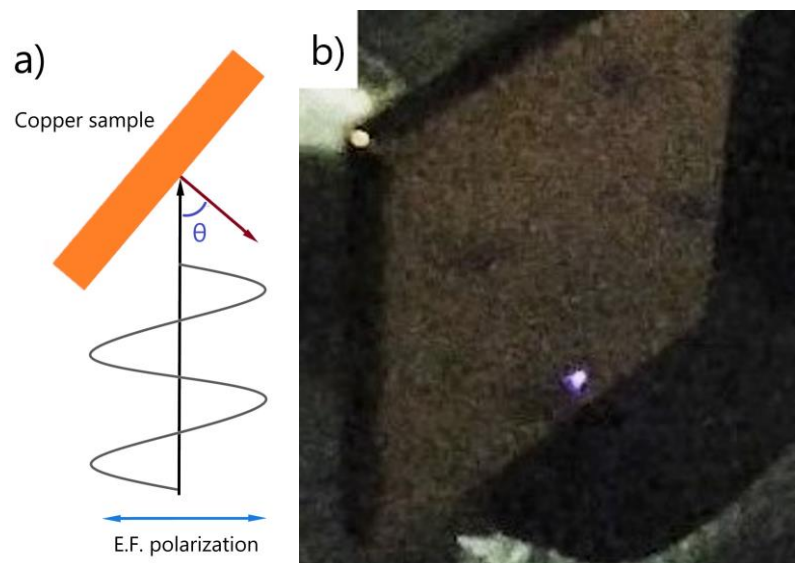
where the micro-pulse intensity  $I_{\text{THz}}$  is

$$I_{\text{THz}} = \frac{W_{\text{THz}}}{\tau \pi r^2} \quad (2)$$

with  $W_{\text{THz}}$  the micro pulse energy,  $\tau$  the micro-pulse time duration, and  $r$  the beam Gaussian waist. In our experiment, irradiations have been carried out on 5 mm thick oxygen-free and high thermal conductivity (OFHC) copper samples, polished down to a nominal roughness (rms)  $< 5$  nm. Each irradiation, composed of 5000 pulses with the total fluence of 635 J/cm<sup>2</sup>, has been delivered in  $\sim 15$  min. The visible damage on the copper surface has been evaluated with a combined optical and chemical analysis. Images have been collected at different magnifications with a scanning electron microscope "Nanoimages MINI-SEM SNE-3200M", while Raman maps have been collected using the JASCO N5100 Optical and Raman microscope.

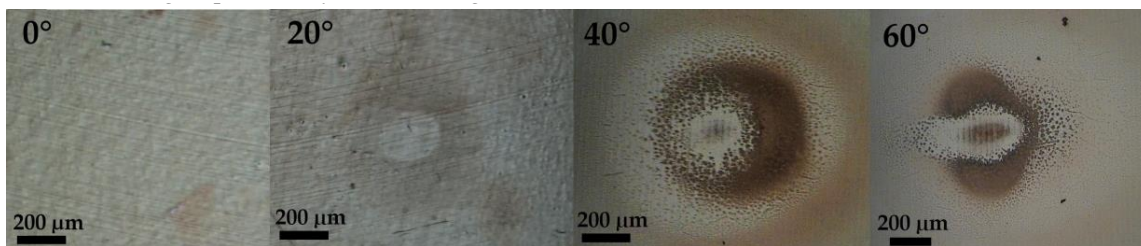
### 3. Results and Discussions

The irradiations have been performed at different angles of incidence, rotating the copper sample from the normal incidence position ( $0^\circ$ ) up to  $60^\circ$ . As shown in Figure 2a, the rotation axis of the sample is perpendicular to the horizontal plane, i.e., normal to the polarization plane of the electric field. During the irradiations, breakdowns phenomena occur in air near the sample surface (Figure 2b).

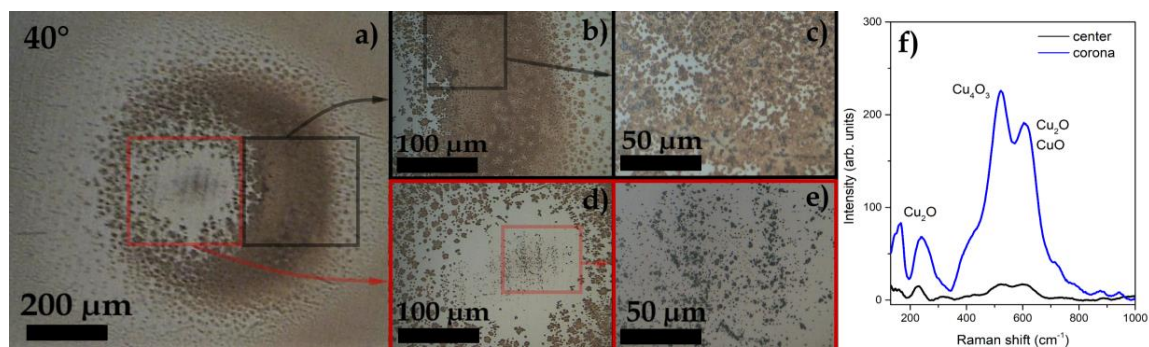


**Figure 2.** (a) Layout of the experimental irradiation at the incidence angle  $\theta$ . The linear polarized radiation hits the copper surface oriented at the selected angle. (b) Image of a spark (bright spot) near the bottom edge occurring on the copper surface irradiated at the incidence angle of  $40^\circ$ .

Figure 3 shows the optical images of the surface damage. In this figure, four optical images taken at different angles after exposition with 5000 pulses are highlighted. At normal incidence, no damage is detectable, while increasing the incidence angle a pattern with evident surface changes appears. This suggests that different phenomena may occur during the irradiation. At this frequency regime, during irradiation, both thermo-mechanical stress and strains are expected to contribute to the surface damage [9]. Using the Raman microscope, we were able to analyze and compare different areas in the damaged regions (see Figure 4). The measurements were performed with a red laser (738 nm) using a spot of  $\sim 1 \mu\text{m}$  ( $100\times$  magnification).



**Figure 3.** Comparison among optical images of the irradiated copper surface taken at different angles of incidence.



**Figure 4.** (a)  $5\times$  magnified image of the damaged region irradiated at  $40^\circ$  after 5000 shots. A central opaque area, an intermediate lighter area, and a dark corona can be recognized. The two squares highlight the  $20\times$  magnified region of the corona (black, panel b) and the central area (red, panel d). The brown corona is due to the oxidation of the copper surface ( $100\times$  magnification in panel c). A  $100\times$  magnification of the central area is highlighted in (panel e). (f) Comparison of the Raman spectra collected in the two magnified areas showing the copper oxides vibrational peaks (mainly CuO and  $\text{Cu}_4\text{O}_3$ ) in the corona and a small presence of oxides in the central region.

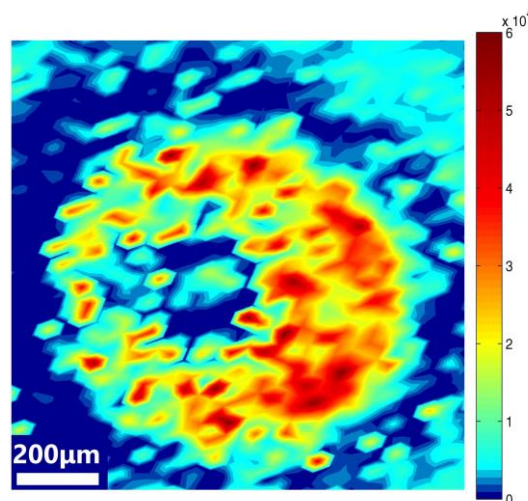
Looking at Figure 4a, two sub-regions in the damaged area can be distinguished: the center, where the THz electric field reaches its maximum intensity and the corona, with an outer diameter of  $\sim 500 \mu\text{m}$ . The analysis of the optical images and the comparison of the different Raman spectra (Figure 4f) suggest that the surface in the corona region contains copper oxides (mainly  $\text{Cu}_4\text{O}_3$  and CuO) [32,33], while the center is almost metallic with a weak contribution of copper oxides [32].

In experiments where coherent radiation interacts with a solid system, the fluence shows a threshold value for the generation of plasma on the surface that depends on the wavelength [34]. The measured plasma generation threshold for copper is  $<2 \text{ J/cm}^2$  at  $1 \mu\text{m}$ , decreasing at longer wavelengths [34]. At this fluence, the irradiation is expected to produce plasma plumes, possibly containing electrons, ions, atoms, molecules, and micro-sized particles, whose dynamics contribute to shaping the damaged pattern [34]. The lack of copper oxide in the central region could be associated with the ablation mechanism induced by the intense THz radiation beam, which continuously removes, at each pulse, part of the oxide layer present on top of the surface.

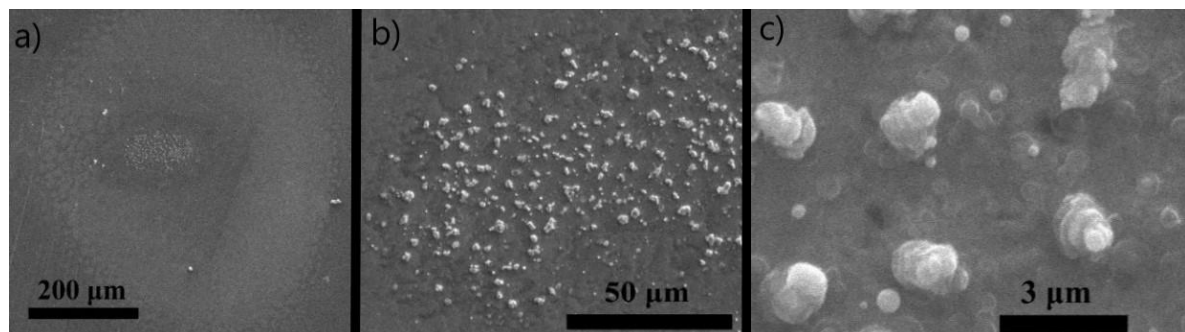
The spatial distribution of copper oxides is shown in Figure 5. This map describes the copper surface irradiated at  $40^\circ$  and has been obtained collecting a grid of  $200 \times 200$  Raman spectra with a



5  $\mu\text{m}$  spot. It allows to reconstruct the spatial distribution of the copper oxides by integrating, in each of the 40000 Raman spectra, the region from 350 to 800  $\text{cm}^{-1}$ , which is associated with CuO and Cu<sub>2</sub>O [32]. As already shown in Figure 4f, the corona has the highest concentration of oxides, while in the central region, they are negligible. A further investigation of the pattern has been obtained through SEM microscopy. Three magnified SEM images of the copper surface are shown in Figure 6 at 40° of incidence. The image on the left shows the two regions: The corona well separated by the dark external copper surface.



**Figure 5.** Raman map of the copper oxide contributions related to the copper surface exposed at 40°, and obtained integrating the range 350–800  $\text{cm}^{-1}$ . The color bar on the right gives the intensity of the integrated Raman signal.



**Figure 6.** Comparison of SEM images of the irradiated copper surface at the angle of incidence of 40°. By increasing the magnification (from left to right), it is possible to recognize in the central area (a), where the highest damage occurs, the presence of hundreds of copper tips (b). Their presence (see magnified tips in (c)) suggests that in this region, it is possible to reach temperatures comparable to higher than the Cu melting point ( $\sim 1085$  °C).

The most intriguing result of the irradiation we performed with ISIR appears in the center of the pattern, where small structures emerge. Their shape and appearance are highlighted in panel c of Figure 6. In order to generate such microstructures, the central area should be exposed to extreme heat with a possible melting of the upper layers in order to form upward pillars. Similar processes might also emerge from surface instabilities on a rigid substrate, leading to self-organization phenomena and the formation of well-organized nano-micro patterns such as the pillar-like structures shown in Figure 6c [35].

Irradiations have also been performed with a lower number of pulses, resulting in different damaging behaviors. For instance, with an irradiation of 500 pulses no damage could have been

resolved on the copper surface at all incidence angles. The result suggests the occurrence of a cumulative thermal effect, most likely a positive feedback process where the growing temperature modifies the absorption efficiency of the surface. Therefore, the rise of the surface temperature is expected for longer exposition times with stronger damage. A similar build-up effect has also been observed in the optical range, as suggested in [36], where a similar behavior of the copper reflectance has been observed when copper was irradiated by multiple intense optical pulses.

Regarding the observed angular dependence, a similar process has been described in the optical range by Miyasaka et al. [37]. Increasing the incidence angle, he revealed for a *p*-polarized high-intensity pulsed laser, a further increase in the absorbance of the copper surface. This latter phenomenon can be modeled through the well-known complex Fresnel equations. The reflected incident radiation with *p*-polarized light has to take into account the complex form:

$$R_p(\theta) = \left[ \frac{-\tilde{n}_{Cu}^2 \cos \theta_i - \sqrt{\tilde{n}_{Cu}^2 - \sin^2 \theta_i}}{\tilde{n}_{Cu}^2 \cos \theta_i + \sqrt{\tilde{n}_{Cu}^2 - \sin^2 \theta_i}} \right]^2 \quad \tilde{n}_{Cu} = n_{Cu} + ik_{Cu} \quad (3)$$

where  $\tilde{n}_{Cu}$  is the complex copper refractive index at ~4 THz [38] and  $\theta_i$  is the incidence angle. From this equation, we may obtain the absorbed fluence  $F_{abs}$  by the copper surface as a function of the incidence angle. The incidence fluence can be written as

$$F = \frac{E_{micro}}{A}; \quad A = \frac{\pi r^2}{\cos \theta_i} \quad (4)$$

where  $E_{micro}$  is the energy of a single micro-pulse and  $A$  the angle-dependent irradiated area. Indeed, when the beam hits the surface, the irradiated area widens with the angle  $\theta_i > 0$ . As a consequence, the fluence absorbed by the surface is

$$F_{abs} = (1 - R_p(\theta)) \cdot F = (1 - R_p(\theta)) \cdot \frac{E_{micro} \cos \theta_i}{\pi r^2} \quad (5)$$

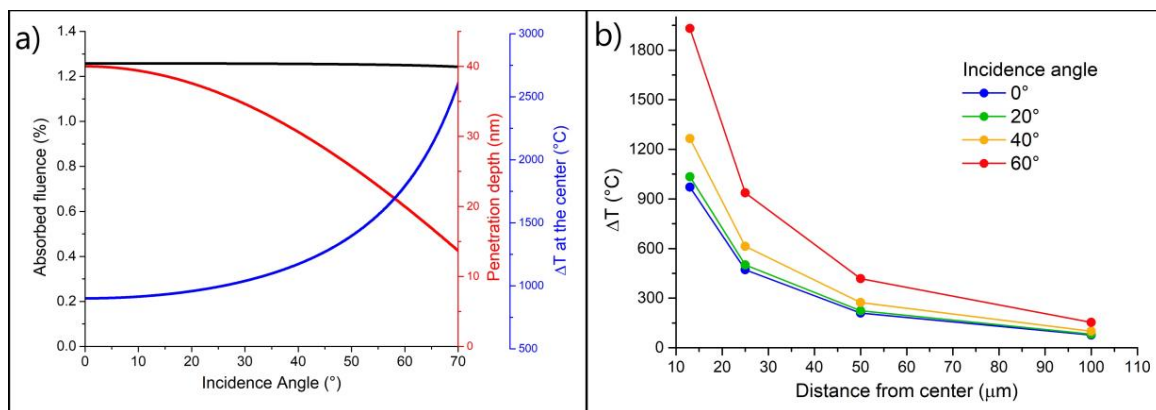
which gives an increase in the temperature:

$$\Delta T = \frac{F_{abs}}{\rho C \delta_{eff}} \quad (6)$$

where  $\rho = 8.96 \text{ g/cm}^3$  is the copper density at room temperature (RT),  $C = 0.385 \text{ J/g } ^\circ\text{C}$  the specific heat capacity at RT and  $\delta_\theta = \delta_0 \cdot \cos \theta_i$  is the penetration depth of the radiation in bulk copper. The latter depends on the angle [39], and  $\delta_0 \sim 40 \text{ nm}$  is the penetration depth at normal incidence in this frequency domain [40]. We obtain the equation:

$$\Delta T_\theta = (1 - R_p(\theta)) \cdot \frac{E_{micro}}{\pi r^2 \rho C \delta_0} = (1 - R_p(\theta)) \cdot \Delta T_{0^\circ} \quad (7)$$

The non-homogenous distribution of the radiation inside the spot determines a gradient in the temperature distribution going from the center to the corona region. Figure 7a shows the angular dependence of the absorbed fluence  $F_{abs}$  (Equation (5), black), the penetration depth (red), and the temperature increase at the center of the spot (Equation (7), blue). Figure 7b describes the  $\Delta T$  vs. the radial distance from the center, for different incidence angles (Equation (7)). If we consider the center of the spot, at angles higher than  $20^\circ$ , the temperature increases more than the melting point of copper ( $\sim 1085^\circ\text{C}$ ), while at  $60^\circ$  the temperature increases above  $1800^\circ\text{C}$ .



**Figure 7.** (a) Angular dependence of the absorbed fluence  $F_{\text{abs}}$  (black), penetration depth (red line), and the temperature increase at the center of the spot. (b)  $\Delta T$  as a function of the distance from the center of the spot at different incidence angles.

#### 4. Conclusions

In this work, we showed for the first time the occurrence of an angular dependent reproducible damage induced by THz multiple high-intensity pulses on metallic copper surfaces. We showed that the damage increases for increasing incidence angles with multiple shots ( $>10^3$ ) and the fluence of  $12.7 \text{ J/cm}^2$  per pulse. We estimated the increase of the temperature of the copper surface with a simple model that reasonably matches the experimental results. It suggests that the increase in absorption at high incidence angles may cause damage and oxidation. The model showed that for incidence angles  $>20^\circ$ , the final temperature can be higher than the melting temperature of copper. The observed damage is in agreement with previous reports in the optical frequency range, described in terms of higher absorbance, increased angle of incidence [36], and multiple shots irradiation [37].

The phenomenology behind the damaging effects can be explained in terms of a fast local temperature increase. It may induce ablation and copper melting on the surface. However, such a description does not consider electric-related effects, e.g., discharges and/or breakdowns occurring in air due to pulses (Figure 2). The breakdown phenomenon occurring at the copper surface is due to the strong electric field applied (estimated  $\sim 4 \text{ GV/m}$ ) in the central region. Actually, pillars formed in the central region could be related to surface instabilities due to both thermal and electric phenomena. In fact, tips could be generated by the coalescence of the melted copper in the central region, or generated during the strong electric field, during which tips act as point-like structures capable of enhancing local electric fields [41].

This work also points out the possibility to use multiple fast irradiations and high-fluence THz radiation to test in a controlled way the damage induced to small areas of a metallic surface by strong electric fields, i.e., in the range of  $4 \text{ GV/m}$ . The results also point out the need to characterize better the observed damage patterns and their dynamics following multiple irradiation procedures. This original approach represents an innovative method to test in a reliable and controlled way the damage induced on a smooth surface. The method offers many potential applications in different technologies and studies, e.g., the construction of accelerating cavities and RF devices.

**Author Contributions:** Conceptualization, methodology, S.M., A.M., A.I. and S.L.; data analysis, S.M., L.T., S.J.R., S.T. and A.M.; Manuscript preparation: S.M., A.M. and L.T.; S.M., L.T., S.J.R., A.M., S.T., A.I., L.F., S.L. have reviewed the manuscript. All authors have read and agreed to the published version of the manuscript.

**Funding:** We acknowledge the financial support of the Bilateral Cooperation Agreement between Italy and Japan of the Italian Ministry of Foreign Affairs and of the International Cooperation (MAECI) in the framework of the project of major relevance N. PGR0072. This work was also supported by “Dynamic Alliance for Open Innovation Bridging Human, Environment and Materials” from the Ministry of Education, Culture, Sports, Science and Technology of Japan (MEXT).

**Acknowledgments:** We acknowledge the INFN for the support within DEMETRA and NUCLEAAR, two projects funded by the INFN Vth Committee. We also acknowledge the Osaka University for providing beamtime at the ISIR facility.

**Conflicts of Interest:** The authors declare no conflict of interest.

## References

1. Jee, Y.; Becker, M.F.; Walser, R.M. Laser-induced damage on single-crystal metal surfaces. *J. Opt. Soc. Am. B* **1988**, *5*, 648. [[CrossRef](#)]
2. Forno, M.D.; Dolgashev, V.; Bowden, G.; Clarke, C.; Hogan, M.; McCormick, D.; Novokhatski, A.; O’Shea, B.; Spataro, B.; Weathersby, S.; et al. High gradient tests of metallic mm-wave accelerating structures. *Nucl. Instrum. Methods Phys. Res. Sect. A* **2017**, *864*, 12–28. [[CrossRef](#)]
3. Forno, M.D.; Dolgashev, V.; Bowden, G.; Clarke, C.; Hogan, M.; McCormick, D.; Novokhatski, A.; O’Shea, B.; Spataro, B.; Weathersby, S.; et al. Measurements of electron beam deflection and RF breakdown rate from a surface wave guided in metallic mm-wave accelerating structures. *Phys. Rev. Accel. Beams* **2018**, *21*, 091301. [[CrossRef](#)]
4. Baston, T.J.; Bowden, F.P. Localized Damage of Metal Crystals by Laser Irradiation. *Nature* **1968**, *218*, 150–152. [[CrossRef](#)]
5. Fedosejevs, R.; Ottmann, R.; Sigel, R.; Kühnle, G.; Szatmári, S.; Schäfer, F.P. Absorption of subpicosecond ultraviolet laser pulses in high-density plasma. *Appl. Phys. B* **1990**, *50*, 79–99. [[CrossRef](#)]
6. Agranat, M.B.; Andreev, N.E.; Ashitkov, S.I.; Veisman, M.E.; Levashov, P.R.; Ovchinnikov, A.V.; Sitnikov, D.S.; Fortov, V.E.; Khishchenko, K.V. Determination of the transport and optical properties of a nonideal solid-density plasma produced by femtosecond laser pulses. *JETP Lett.* **2007**, *85*, 271–276. [[CrossRef](#)]
7. Ng, A.; Celliers, P.; Forsman, A.; More, R.M.; Lee, Y.T.; Perrot, F.; Dharma-Wardana, M.W.C.; Rinker, G.A. Reflectivity of intense femtosecond laser pulses from a simple metal. *Phys. Rev. Lett.* **1994**, *72*, 3351. [[CrossRef](#)]
8. Cerchez, M.; Jung, R.; Osterholz, J.; Toncian, T.; Willi, O.; Mulser, P.; Ruhl, H. Absorption of ultrashort laser pulses in strongly overdense targets. *Phys. Rev. Lett.* **2008**, *100*, 245001. [[CrossRef](#)]
9. Agranat, M.B.; Chefonov, O.V.; Ovchinnikov, A.V.; Ashitkov, S.I.; Fortov, V.E. Damage in a thin metal film by high-power terahertz radiation. *Phys. Rev. Lett.* **2018**, *120*, 085704. [[CrossRef](#)]
10. Tan, P.; Huang, J.; Liu, K.; Xiong, Y.; Fan, M. Terahertz radiation sources based on free electron lasers and their applications. *Sci. China Inf. Sci.* **2012**, *55*, 1–15. [[CrossRef](#)]
11. Rezvani, J.; Di Gioacchino, D.; Gatti, C.; Poccia, N.; Ligi, C.; Tocci, S.; Guidi, M.C.; Cibella, S.; Lupi, S.; Marcelli, A. Tunable vortex dynamics in proximity junction arrays: A possible accurate and sensitive 2D THz detector. *Acta Phys. Pol. A* **2020**, *137*, 17–20. [[CrossRef](#)]
12. Tonouchi, M. Cutting-edge terahertz technology. *Nat. Photon.* **2007**, *1*, 97–105. [[CrossRef](#)]
13. Chiadroni, E.; Bacci, A.; Bellaveglia, M.; Boscolo, M.; Castellano, M.; Cultrera, L.; Di Pirro, G.; Ferrario, M.; Ficcadenti, L.; Filippetto, D.; et al. The SPARC linear accelerator based terahertz source. *Appl. Phys. Lett.* **2013**, *102*, 094101. [[CrossRef](#)]
14. Chiadroni, E.; Bellaveglia, M.; Calvani, P.; Castellano, M.; Catani, L.; Cianchi, A.; Di Pirro, G.; Ferrario, M.; Gatti, G.; Limaj, O.; et al. Characterization of the THz radiation source at the Frascati linear accelerator. *Rev. Sci. Instrum.* **2013**, *84*, 022703. [[CrossRef](#)]
15. Perucchi, A.; Di Mitri, S.; Penco, G.; Allaria, E.; Lupi, S. The TeraFERMI terahertz source at the seeded FERMI free-electron-laser facility. *Rev. Sci. Instrum.* **2013**, *84*, 022702. [[CrossRef](#)]
16. Lupi, S.; Nucara, A.; Perucchi, A.; Calvani, P.; Ortolani, M.; Quaroni, L.; Kiskinova, M. Performance of SISSI, the infrared beamline of the ELETTRA storage ring. *J. Opt. Soc. Am. B* **2007**, *24*, 959. [[CrossRef](#)]
17. Rezvani, S.J.; Pinto, N.; Enrico, E.; D’Ortenzi, L.; Chiodoni, A.; Boarino, L. Thermally activated tunneling in porous silicon nanowires with embedded Si quantum dots. *J. Phys. D Appl. Phys.* **2016**, *49*, 105104. [[CrossRef](#)]
18. Pinto, N.; Rezvani, S.J.; Perali, A.; Flammia, L.; Milošević, M.V.; Fretto, M.; Cassiago, C.; De Leo, N. Dimensional crossover and incipient quantum size effects in superconducting niobium nanofilms. *Sci. Rep.* **2018**, *8*, 4710. [[CrossRef](#)]



19. Pinto, N.; Rezvani, S.J.; Favre, L.; Berbezier, I.; Fretto, M.; Boarino, L. Geometrically induced electron-electron interaction in semiconductor nanowires. *Appl. Phys. Lett.* **2016**, *109*, 123101. [[CrossRef](#)]
20. Rezvani, S.J.; Perali, A.; Fretto, M.; De Leo, N.; Flammia, L.; Milošević, M.; Nannarone, S.; Pinto, N. Substrate-Induced Proximity Effect in Superconducting Niobium Nanofilms. *Condens. Matter* **2019**, *4*, 4. [[CrossRef](#)]
21. Ortolani, M.; Lupi, S.; Baldassarre, L.; Schade, U.; Calvani, P.; Takano, Y.; Nagao, M.; Takenouchi, T.; Kawarada, H. Low energy electrodynamics of superconducting diamonds. *Phys. Rev. Lett.* **2006**, *97*, 097002. [[CrossRef](#)] [[PubMed](#)]
22. Zhang, X.-C.; Ma, X.F.; Jin, Y.; Lu, T.-M. Terahertz optical rectification from a nonlinear organic crystal. *Appl. Phys. Lett.* **1992**, *61*, 3080–3082. [[CrossRef](#)]
23. Zhang, X.; Jin, Y.; Ma, X.F. Coherent measurement of THz optical rectification from electro-optic crystals. *Appl. Phys. Lett.* **1992**, *61*, 2764–2766. [[CrossRef](#)]
24. Winnerl, S.; Stehr, D.; Drachenko, O.; Schneider, H.; Helm, M.; Seidel, W.; Michel, P.; Schneider, S.; Seidel, J.; Grafstrom, S.; et al. FELBE Free-Electron Laser: Status and application for time resolved spectroscopy experiments. In Proceedings of the 2006 Joint 31st International Conference on Infrared Millimeter Waves and 14th International Conference on Terahertz Electronics, Shanghai, China, 18–22 September 2006.
25. Kato, R.; Kashiwagi, S.; Morio, Y.; Furuhashi, K.; Terasawa, Y.; Sugimoto, N.; Suemine, S.; Isoyama, G. High power terahertz FEL at ISIR, Osaka University. In Proceedings of the IPAC'10, Kyoto, Japan, 23–28 May 2010.
26. Nanni, E.A.; Huang, W.R.; Hong, K.; Ravi, K.; Fallahi, A.; Moriena, G.; Miller, R.J.D.; Kärtner, F.X. Terahertz-driven linear electron acceleration. *Nat. Commun.* **2015**, *6*, 8486. [[CrossRef](#)]
27. Boni, R.; Chimenti, V.; Spataro, B.; Tazzioli, F.; Fernandes, P.; Parodi, R. Design and operation of a multipacting-free 51.4 MHz RF accelerating cavity. *Nucl. Instrum. Methods Phys. Res.* **1989**, *274*, 49–55. [[CrossRef](#)]
28. Macis, S.; Rezvani, J.; Davoli, I.; Cibir, G.; Spataro, B.; Scifo, J.; Faillace, L.; Marcelli, A. Structural Evolution of MoO<sub>3</sub> Thin Films Deposited on Copper Substrates upon Annealing: An X-ray Absorption Spectroscopy Study. *Condens. Matter* **2019**, *4*, 41. [[CrossRef](#)]
29. Macis, S.; Aramo, C.; Bonavolontà, C.; Cibir, G.; D'Elia, A.; Davoli, I.; De Lucia, M.; Lucci, M.; Lupi, S.; Miliucci, M.; et al. MoO<sub>3</sub> films grown on polycrystalline Cu: Morphological, structural and electronic. *J. Vac. Sci. Technol. A* **2019**, *37*, 021513. [[CrossRef](#)]
30. Kwan, T.; Dawson, J.M.; Lin, A.T. Free electron laser. *Phys. Fluids* **1977**, *20*, 581. [[CrossRef](#)]
31. Irizawa, A.; Suga, S.; Nagashima, T.; Higashiya, A.; Hashida, M.; Sakabe, S. Laser-induced fine structures on silicon exposed to THz-FEL. *Appl. Phys. Lett.* **2017**, *111*, 251602. [[CrossRef](#)]
32. Bommireddy, P.R.; Sivajee-Ganesh, K.; Jayanth-Babu, K.; Hussain, O.M.; Julien, C.M. Microstructure and supercapacitive properties of RF-sputtered copper oxide thin films: Influence of O<sub>2</sub>/Ar ratio. *Ionics* **2015**, *21*, 2319–2328.
33. Levitskii, V.S.; Shapovalov, V.I.; Komlev, A.E.; Zav'yalov, A.V.; Vit'ko, V.V.; Komlev, A.A.; Shutova, E.S. Raman spectroscopy of copper oxide films deposited by reactive magnetron sputtering. *Tech. Phys. Lett.* **2015**, *41*, 1094–1096. [[CrossRef](#)]
34. Butt, M.Z. Laser ablation characteristics of metallic materials: Role of Debye-Waller thermal parameter. In Proceedings of the IOP Conference Series: Materials Science and Engineering, Metz, France, 30 June–4 July 2014; Volume 60, p. 012068.
35. Antoine, C.Z.; Peauger, F.; Le Pimpec, F. Electromigration occurrences and its effects on metallic surfaces submitted to high electromagnetic field: A novel approach to breakdown in accelerators. *Nucl. Instrum. Methods Phys. Res. Sect. A* **2011**, *665*, 54–69. [[CrossRef](#)]
36. Vorobyev, A.Y.; Guo, C. Reflection of femtosecond laser light in multipulse ablation of metals. *J. Appl. Phys.* **2011**, *110*, 043102. [[CrossRef](#)]
37. Miyasaka, Y.; Hashida, M.; Nishii, T.; Inoue, S.; Sakabe, S. Derivation of effective penetration depth of femtosecond laser pulses in metal from ablation rate dependence on laser fluence, incidence angle, and polarization. *Appl. Phys. Lett.* **2015**, *106*, 013101. [[CrossRef](#)]
38. Hagemann, H.J.; Gudat, W.; Kunz, C. Optical constants from the far infrared to the x-ray region: Mg, Al, Cu, Ag, Au, Bi, C, and Al<sub>2</sub>O<sub>3</sub>. *J. Opt. Soc. Am.* **1975**, *65*, 742. [[CrossRef](#)]
39. Liao, Y.-C.; Yu, M.-H. Effects of laser beam energy and incident angle on the pulse laser welding of stainless steel thin sheet. *J. Mater. Process. Technol.* **2007**, *190*, 102–108. [[CrossRef](#)]

40. Rakić, A.D.; Djurišić, A.B.; Elazar, J.M.; Majewski, M.L. Optical properties of metallic films for vertical-cavity optoelectronic devices. *Appl. Opt.* **1998**, *37*, 5271–5283. [[CrossRef](#)]
41. Grudiev, A.; Calatroni, S.; Wuensch, W. New local field quantity describing the high gradient limit of accelerating structures. *Phys. Rev. Spec. Top. Accel. Beams* **2009**, *12*, 102001. [[CrossRef](#)]



© 2020 by the authors. Licensee MDPI, Basel, Switzerland. This article is an open access article distributed under the terms and conditions of the Creative Commons Attribution (CC BY) license (<http://creativecommons.org/licenses/by/4.0/>).